6th European Conference on Computational Mechanics (ECCM 6)
7th European Conference on Computational Fluid Dynamics (ECFD 7)
1115 June 2018, Glasgow, UK

A FLUID-STRUCTURE INTERACTION MODEL BASED ON PERIDYNAMICS AND NAVIER-STOKES EQUATIONS FOR HYDRAULIC FRACTURE PROBLEMS

F. DALLA BARBA[1], P. CAMPAGNARI[2], M. ZACCARIOTTO[2], U. GALVANETTO[2] AND F. PICANO[2]

[1] CISAS, University of Padova
Via Venezia 15, 35131, Padova, Italy
federico.dallabarba@phd.unipd.it

[2] Department of Industrial Engineering, University of Padova
Via Venezia 1, 35131, Padova, Italy

Key words: Fluid-structure interaction, peridynamics, immersed boundary method

Abstract. The interaction among fluid flows and solid structures is a complex nonlinear phenomenon that is of crucial importance in a wide range of scientific and engineering contexts. Nevertheless, simple analytical solutions of the governing equations are often not possible to obtain and critical difficulties arise also numerically attacking the problem. A wide range of methodologies can be found in archival literature to approach fluid-structure interaction (FSI) problems. Within these, a particularly challenging matter deals with the reproduction of the dynamics of solid media fracture due to the action of hydrodynamic forces, i.e. the hydraulic fracture. An example consists in the fracking process, adopted to extract gas from shale rocks. In this context, the present work aims to investigate the capabilities of a novel numerical method to reproduce solid fragmentation within fluid media. The proposed method is based on peridynamic equations coupled with Navier-Stokes equations through an immersed boundary method (IBM). The main advantages introduced by peridynamics consist in the natural crack detection and the automatic tracking of crack propagation. The proposed FSI method has been implemented into a parallel code. The temporal integration is performed by an explicit third-order Runge-Kutta algorithm; Navier-Stokes equations are discretized by second-order finite differences and coupled with the multidirect IBM algorithm to account for fluid-solid force exchange. Preliminary tests on simple configurations show the ability of the method to solve fluid-structure interaction problems with possible crack formations.

1 INTRODUCTION

Fluid-structure interaction problems [1] are involved in a variety of engineering applications and scientific fields ranging from aeroelasticity [2] to the interaction between fluid and cells in biological flows [3, 4]. A particularly challenging topic is that of solid media fracture within fluids, i.e. the fracking process adopted to extract gas from shale rocks [5]. Due to the strong non-linearity and multidisciplinary nature of FSI problems, few can be done approaching the problems by a theoretical point of view and even numerical simulations can be extremely challenging. In this context, the present work aims to investigate the capabilities of a novel numerical method to reproduce solid fragmentation within fluid media. Solid mechanics is described in the framework of peridynamics [6]. In this formulation of continuum mechanics the interaction among material points is described by integral equations. The main advantages introduced by this approach is achieved when crack formation is accounted for [7]. Indeed, in these cases local theories may present issues due to singularity of derivatives in partial differential equations. Conversely, the use of integral equations can avoid the onset of this kind of problem when crack formation occurs. In order to reproduce the solid-liquid interaction several methods have been proposed in archival literature. When complex and time-evolving interfaces are considered, immersed boundary methods are powerful tools capable to mimic no-slip and no-penetration boundary conditions. The basic principle behind IBM is that of imposing an additional forcing in the fluid, within a neighbourhood of fluid-solid interface, such that the wall boundary conditions are satisfied within certain accuracy. The present work uses a multidirect IBM algorithm to account for fluid-solid force exchange. The incompressible formulation of the Navier-Stokes equations governs the fluid dynamics while a full coupling with peridynamic equation of motion is achieved through the IBM algorithm. The proposed methodology has been implemented into a massively parallelized Fortran code. Some validation test cases and preliminary results are provided.

2 NUMERICAL METHOD AND MODEL

Peridynamics is a non-local continuum theory [6] based on the assumption that material points interact among each other within a given threshold distance, δ, called peridynamic *horizon*. In the so called *bond-based* formulation of peridynamics interactions occurs between couples of material points and each interaction, referred to as *bond*, is assumed to be independent from each other. Let $\mathcal{B}$ be the reference configuration of a solid body such that $\boldsymbol{X}_0 \in \mathcal{B}$ is the coordinate of each material point in the reference configuration. Let then consider a motion of the body such that $\boldsymbol{X}(\boldsymbol{X}_0, t)$ is the Lagrangian coordinate of the material point with initial position $\boldsymbol{X}_0$ at time $t \geq 0$. Hence, the motion of each material point can be described by the following integral equation [8]:

$$\rho_s \frac{d^2\boldsymbol{X}(\boldsymbol{X}_0, t)}{dt^2} = \int_{\mathcal{H}_{\boldsymbol{X}_0}} \boldsymbol{f}\left[\boldsymbol{X}'(\boldsymbol{X}'_0, t) - \boldsymbol{X}(\boldsymbol{X}_0, t), \boldsymbol{X}'_0 - \boldsymbol{X}_0\right] dV_{\boldsymbol{X}'_0} + \boldsymbol{B}(\boldsymbol{X}_0, t), \tag{1}$$

where ρ_s is the solid media density, the integration domain is a neighbourhood of $\boldsymbol{X}_0$, $\mathcal{H}_{\boldsymbol{X}_0} = \{\boldsymbol{X}'_0 \in \mathcal{B}, ||\boldsymbol{X}'_0 - \boldsymbol{X}_0|| < \delta\}$ and $\boldsymbol{X}'$, $\boldsymbol{X}'_0$ are dummy integration variables representing the coordinates of each material point partaining to $\mathcal{H}_{\boldsymbol{X}_0}$. The vector $\boldsymbol{B}(\boldsymbol{X}_0, t)$

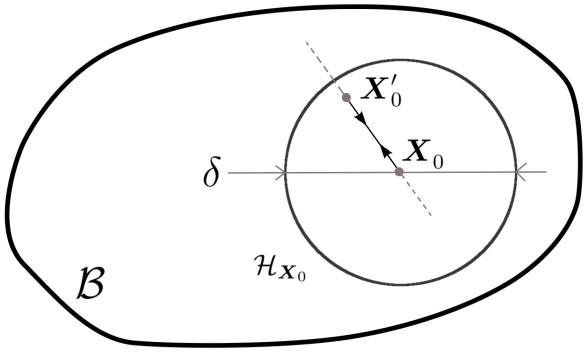

Figure 1: Schematic of peridynamic formulation of continuum mechanics. $\mathcal{B}$ is the reference configuration of the solid media. The peridynamic horizon, δ, defines the family, $\mathcal{H}_{\boldsymbol{X}_o}$, of material points $\boldsymbol{X}'_0$ interacting with the material point $\boldsymbol{X}_0$.

accounts for external force density per unit volume acting on the body. The function $\boldsymbol{f}$, for the sake of simplicity $\boldsymbol{f}(\boldsymbol{X}'_0, \boldsymbol{X}_0, t)$, is called *pairwise force function*. It is a force density per unit volume squared representing the action of material point $\boldsymbol{X}'$ on $\boldsymbol{X}$. In the *bond-based* peridynamic model, due to mutual independence of interactions, the *pair-wise force function* $\boldsymbol{f}(\boldsymbol{X}'_0, \boldsymbol{X}_0, t)$ can be expresses as a function of the relative position of the material points in the reference configuration, $\boldsymbol{\xi}$ and their relative displacement in actual configuration, $\boldsymbol{\eta}$. These assumption holds for the so-called *micro-elastic materials* for which the *pair-wise force function* can be derived from a potential. It is then possible to define:

$$s(\boldsymbol{\xi}, \boldsymbol{\eta}) = \frac{||\boldsymbol{\xi} + \boldsymbol{\eta}|| - ||\boldsymbol{\xi}||}{||\boldsymbol{\xi}||}, \tag{2}$$

$$\boldsymbol{\xi} = \boldsymbol{X}'_0 - \boldsymbol{X}_0, \tag{3}$$

$$\boldsymbol{\eta} = (\boldsymbol{X}' - \boldsymbol{X}'_0) - (\boldsymbol{X} - \boldsymbol{X}_0), \tag{4}$$

with s the bond stretch. Then, under these hypotheses, the pairwise force function can then be expressed as [9] [10]:

$$\boldsymbol{f}(\boldsymbol{\xi}, \boldsymbol{\eta}) = c_0 \ \mu(s) \ s \ \frac{\boldsymbol{\xi} + \boldsymbol{\eta}}{||\boldsymbol{\xi} + \boldsymbol{\eta}||}. \tag{5}$$

The parameter c_0 is called *micro-modulus* and represents the stiffness of the bond. In the present work it is assumed to be constant but dependency from bond position and time can be included. In peridynamics it is assumed that crack occurs via bond rupture when bond stretch overcomes a threshold value, s_0. Hence, the parameter μ is introduced to account for crack formation:

$$\mu(s) = \begin{cases} 1, & s \leq s_0 \quad \forall t \geq 0 \\ 0, & otherwise. \end{cases} \tag{6}$$

The *micro-modulus* can be expressed as [11]:

$$c_0 = \begin{cases} \frac{9E}{\pi h \delta^3}, & 2D\ plane\ stress \\ \frac{48E}{5\pi h \delta^3}, & 2D\ plane\ strain \\ \frac{12E}{\pi \delta^4}, & 3D. \end{cases} \tag{7}$$

The limit bond stretch is a function of the critical fracture energy release rate of the material, G_0 and can be computed from the following relations [12]:

$$s_0 = \begin{cases} \sqrt{\frac{4\pi G_0}{9E\delta}}, & 2D\ plane\ stress \\ \sqrt{\frac{5\pi G_0}{12E\delta}}, & 2D\ plane\ strain \\ \sqrt{\frac{5G_0}{9E\delta}}, & 3D. \end{cases} \tag{8}$$

Equation 1 is numerically solved by a fully explicit, low storage, third order Runge-Kutta algorithm. In order to cut high frequency vibrations and consent the computation of steady solution an additional damping term is added to the right-hand side of the equation. Hence, the discretized form of equation 1 reads:

$$\rho_s \frac{d^2 \boldsymbol{X}_i}{dt^2} = \sum_{j=1}^{N_i} \left[c_0\ \mu(s_{i,j})\ s_{i,j}\ \frac{\boldsymbol{\xi}_{i,j} + \boldsymbol{\eta}_{i,j}}{||\boldsymbol{\xi}_{i,j} + \boldsymbol{\eta}_{i,j}||}. \right] \Delta V_j - k_d(\boldsymbol{U}_i - \boldsymbol{U}_{avg,i}) + \boldsymbol{B_i}, \tag{9}$$

where N_i is the number of peridynamic particles pertaining to the neighbourhood of particle i, k_d is a damping coefficient, $\boldsymbol{U}_i$ is the velocity of particle i and $\boldsymbol{U}_{avg,i}$ is the average of the velocities of particles within the neighbourhood of particle i. The external force density $\boldsymbol{B}_i$ represents the time-dependent load applied by the fluid on the solid media surface and will be discussed below.

Concerning the flow solver, the open-source CaNS parallel code, originally developed by P. Costa [17], has been adopted and expanded with the Immersed Boundary Method of [13]. In more detail, the Navier-Stokes equations for a Newtonian incompressible fluid are:

$$\nabla \cdot \boldsymbol{u} = 0, \tag{10}$$

$$\rho_f \left(\frac{\partial \boldsymbol{u}}{\partial t} + \boldsymbol{u} \cdot \nabla \boldsymbol{u} \right) = -\nabla p + \mu_f \nabla^2 \boldsymbol{u} + \rho_f \boldsymbol{f}, \tag{11}$$

where $\boldsymbol{u}$ is the velocity, p the hydrodynamic pressure, ρ_f the density and μ_f the dynamic viscosity of the fluid. In the IBM framework, the no-slip and no-penetration conditions are not directly imposed at the solid-fluid interface. Instead, a force per unit mass, $\boldsymbol{f}$, is added to the right-hand side of equation 11 to mimic the boundary conditions. The integration of equations 10 and 11 is also performed through a low storage third order Runge-Kutta method. The solution is advanced via a pressure correction scheme on a fixed, staggered and equispaced Cartesian grid, referred to as Eulerian grid. The pressure

correction scheme applied to the discretized form of equation 11 can be summarized as in the following:

$$\boldsymbol{u}^{*} = \boldsymbol{u}^{n-1} + \frac{\Delta t}{\rho_f}\left[\alpha_n \boldsymbol{RHS}^{n-1} + \beta_n \boldsymbol{RHS}^{n-2} - (\alpha_n + \beta_n)\nabla p^{n-3/2}\right], \tag{12}$$

$$\boldsymbol{u}^{**} = \boldsymbol{u}^{*} + \Delta t \boldsymbol{f}^{n-1/2}, \tag{13}$$

$$\nabla^2 \hat{p} = \frac{\rho_f}{(\alpha_n + \beta_n)\Delta t}\nabla \cdot \boldsymbol{u}^{**}, \tag{14}$$

$$\boldsymbol{u}^{n} = \boldsymbol{u}^{**} - \frac{(\alpha_n + \beta_n)\Delta t}{\rho_f}\nabla \hat{p}, \tag{15}$$

$$p^{n-1/2} = p^{n-3/2} + \hat{p}, \tag{16}$$

where the superscript n referes to the n^{th} step of the Runge-Kutta scheme, Δt is the time step and α_n, β_n are the Runge-Kutta coefficients. The right-hand side term is $\boldsymbol{RHS} = -\rho_f \nabla \cdot (\boldsymbol{uu}) + \mu_f \nabla^2 \boldsymbol{u}$. The velocities $\boldsymbol{u}^{*}$ and $\boldsymbol{u}^{**}$ are the first and second prediction velocities respectively. The IBM forcing, $\boldsymbol{f}$, is introduced after the discretization of equation 11 and is computed iteratively. To this purpose a moving Lagrangian grid located on the fluid-solid interface is considered. The Lagrangian grid nodes are defined by peridynamic material particles located on the fluid-solid interface. The grid moves with the solid-fluid interface such that each node of the grid coincide with the position of each particle, $\boldsymbol{X}_l$, at each time step. In this framework, the IBM forcing is computed according to the following multidirect forcing scheme [13]:

$$\boldsymbol{U}_l^{*,s-1} = \sum_{i,j,k} \boldsymbol{u}_{i,j,k}^{*,s-1} \delta(\boldsymbol{x}_{i,j,k} - \boldsymbol{X}_l^n)\Delta V_e, \tag{17}$$

$$\boldsymbol{F_l}^{n+1/2,s} = \frac{\boldsymbol{U}_l^n - \boldsymbol{U}_l^{*,s-1}}{\Delta t}, \tag{18}$$

$$\boldsymbol{f}_{i,j,k}^{n+1/2,s} = \sum_{l} \boldsymbol{F}_l^{n+1/2,s} \delta(\boldsymbol{x}_{i,j,k} - \boldsymbol{X}_l^n)\Delta V_l, \tag{19}$$

$$\boldsymbol{u}_{i,j,k}^{s} = \boldsymbol{u}_{i,j,k}^{*} + \Delta t \boldsymbol{f}_{i,j,k}^{n+1/2,s}, \tag{20}$$

where the superscript s refers to the s^{th} iteration of the multidirect scheme while n to the n^{th} step of the Runge-Kutta algorithm. The volume ΔV_e is the Eulerian grid volume while ΔV_l is the Lagrangian particle volumes. The Lagrangian velocity $\boldsymbol{U}_l^{*,s-1}$ is computed at each Lagrangian node by the interpolation of the first prediction velocity $\boldsymbol{u}_{i,j,k}^{*,s-1}$ in the neighbouring Eulerian nodes. The forcing $\boldsymbol{F}_l^{n+1/2,s}$ is then computed on the Lagrangian grid by the difference between the interpolated prediction velocity, $\boldsymbol{U}_l^{*,s-1}$ and the peridynamic material particle velocity, $\boldsymbol{U}_l^n$. Finally, the forcing is spread on the Eulerian grid and the prediction velocity is updated. These scheme is iterated until the no-slip, no-penetration conditions are prescribed with arbitrary certain at the solid-fluid interface. The *interpolation* and *spreading* operations are performed via the regularized delta Dirac function, δ_d [14]. At each time step the prediction velocity is computed. Then, the multidirect forcing scheme is used to compute IBM forcing and the prediction

velocity is updated in order to mimic no-slip and no-penetration boundary conditions. At this step a fast Fourier transform solver is used to solve the Poisson equation for pressure. The correction velocity is then computed by projecting the prediction velocity in the divergence-free space. Finally, peridynamic equations are advanced using the IBM forcing computed on the Lagrangian grid, $\boldsymbol{B}_i = \rho_s \boldsymbol{F}_l$

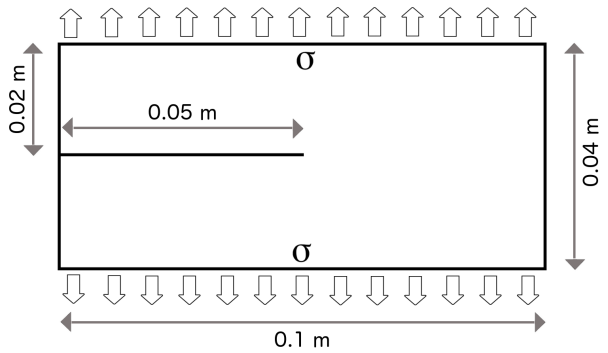

Figure 2: Dimensions of pre-cracked plate. The tensile load, σ, is applied to the upper and lower side of the plate while the left and right sides are free.

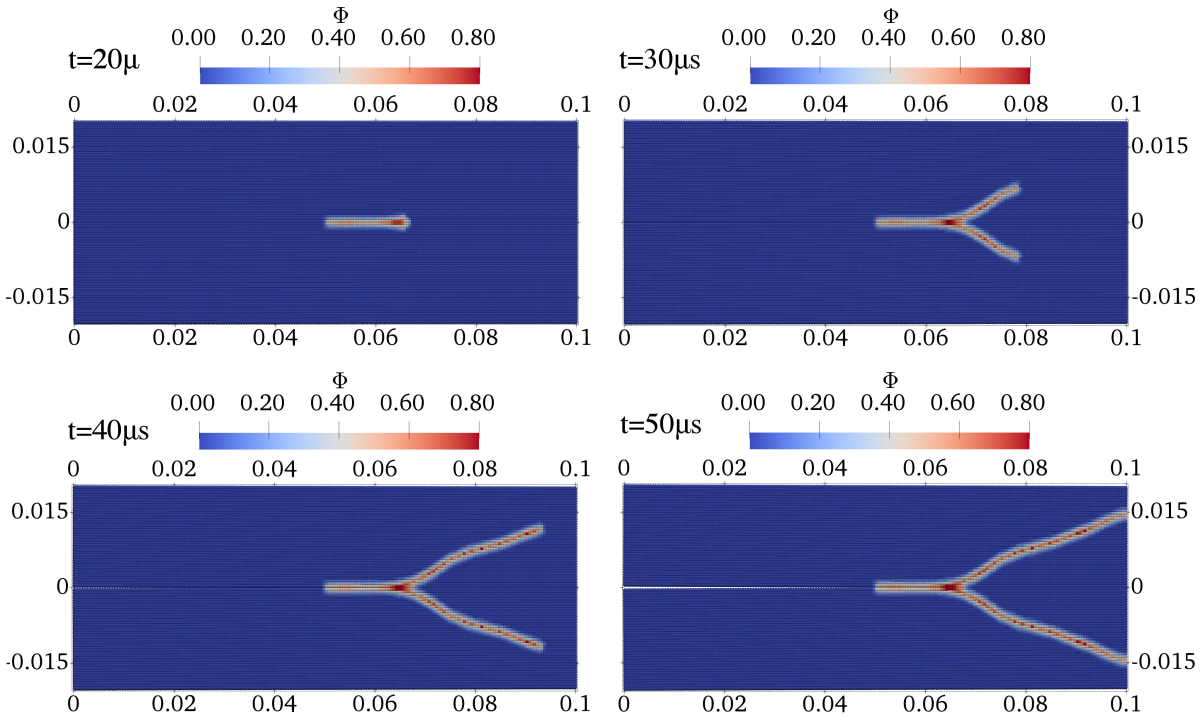

Figure 3: Crack branching in pre-cracked plate at four different time steps. The crack starts to propagate at $t \simeq 10\mu s$ from the tip of the initial notch and reaches the left side of the plate at $t \simeq 50\mu s$. The contour provides the damage level in the material according to equation 21.

3 RESULTS

The described methodology has been implemented into a massively parallelized Fortran code based on MPI and OpenMP directives. Preliminary validation and testing are described below. The first validation test considers only the peridynamic solver and deals with crack branching in a plate with a pre-notch subjected to step load. A tensile load of of $\sigma = 12MPa$ is applied as described in figure 2. The material properties of the plate are set to that of *Soda-Lime glass*, $E = 72GPa$, $\rho_s = 2440kg/m^3$ and $G_0 = 135J/m^2$ where E is the material Young's modulus. The plate is discretized using an equispaced Cartesian distribution of 200×80 particles along the free-edge and loaded directions respectively. The ratio between particle spasing, Δ, and peridynamic horizon, δ, is set to $m = \Delta/\delta = 3$. The simulation is run for $t = 50\mu s$ with a time step of $\Delta t = 50ns$. The results are provided by figure 3 for $t = 20\mu s$, $t = 30\mu s$, $t = 40\mu s$ and $t = 50\mu s$. The figure provides for each time step the contour plot of the damage level, Φ, defined as:

$$\Phi = 1 - \frac{\sum_{i=1}^{N_i} \mu(s_{i,j}) \Delta V_j}{\sum_{i=1}^{N_i} \Delta V_j}. \tag{21}$$

The results are in optimum agreement with that obtained by Dipasquale et al. [7] and Ha et al. [9].

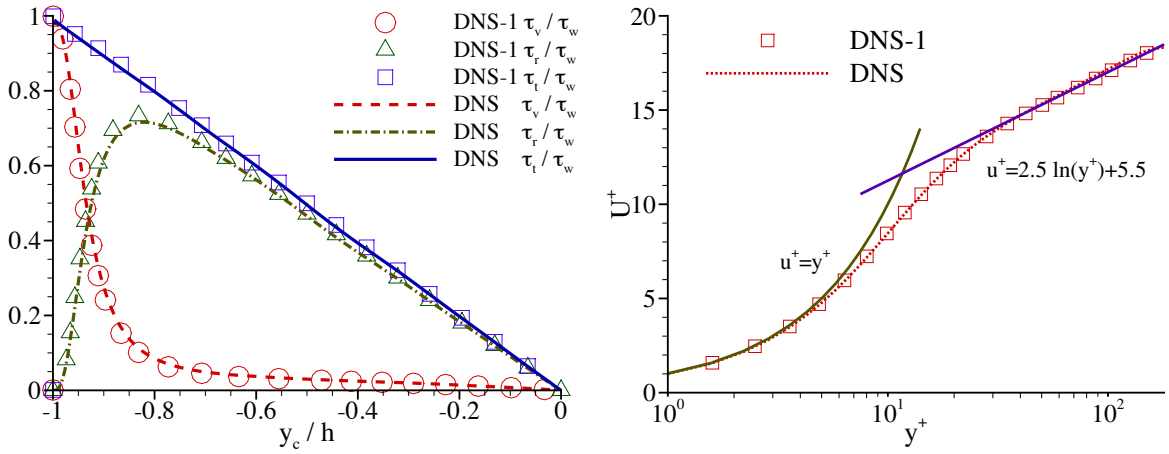

(a) (b)

Figure 4: (a) Reynolds stress $\tau_r = -\rho_f \langle u'v' \rangle$, viscous stress, $\tau_v = \mu_f \partial u/\partial y$ and total shear stress, $\tau_t = \tau_r + \tau_v$ as a function of the distance from the channel centre line, y_c. The stresses are normalized by wall stress, τ_w, while the centre-line-distance is normalized by the channel height, h. The DNS curves reports thhe results of current simulation while the DNS-1 curves provides the numerical results obtained by Kim et al. [15].

The second validation test considers only the fluid solver. The direct numerical simulation (DNS) of a periodic channel flow has been performed and the stress budget and wall law have been considered as the validation targets. The computation is carried out with 3932160 grid nodes, $192 \times 128 \times 160$, in the flow, wall-normal and span-wise directions

respectively. The computational grid extends for $2\pi h \times h \times \pi h$ in the same directions with h the channel height. The bulk Reynolds number based on the inflow bulk velocity is set to $Re_b = U_b h/\nu_f = 5600$ with U_b the bulk velocity and ν_f the kinematic viscosity of the flow. Figure 4(a) provides the Reynolds stress, $\tau_r = -\rho_f \langle u'v' \rangle$, the viscous stress, $\tau_v = \mu_f \partial u/\partial y$ and the total shear stress $\tau_t = \tau_r + \tau_v$ computed as a function of the distance from the centre line of the channel, y_c, in absolute coordinates. All the stresses are non dimensional with the reference scale set to the total shear stress at wall, τ_w. All the statistics are computed after the establishment of a statistical stationary condition in the flow. Mean quantities are averaged over time and the flow and spanwise directions. Figure 4(b) provides the mean velocity on $U^+ = \langle u \rangle / u_\tau$ versus the distance from channel wall, $y^+ = y\ u_\tau/\nu_f$. All quantities are expressed in *wall units* where $u_\tau = \sqrt{\tau_w/\rho_f}$ is the friction velocity and τ_w the wall friction. Figures 4(a) and 4(b) provides also a comparison with the results obtained by Kim et al. [15]. The Reynolds number $Re_\tau = u_\tau h/(2\nu_f)$ obtained from the simulation is $Re_\tau \simeq 180$ which is in optimum agreement with theoretical and previous numerical results. Additional tests on the results accuracy and the scaling performances can be found in [17].

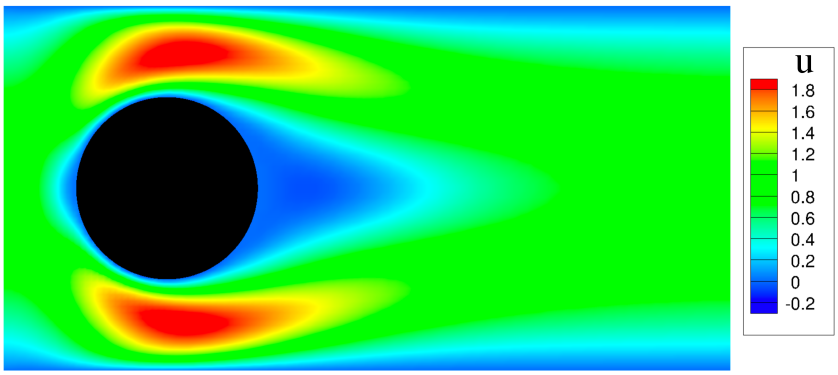

Figure 5: Computational domain of the simulation of a 2D cylinder immersed in a channel flow at $Re_b = U_b h/\nu_f$. The cylinder has a diameter of $d = 1/2h$, with h the channel height. The contour plots the non-dimensional velocity field, $\mathbf{u}$, in stationary conditions with the reference velocity scale set to $U_0 = U_b$.

The last validation test consists of a preliminary small-size simulation considering the IBM algorithm and the fluid solver. The simulation reproduces the flow in a 2D channel extending for $4h \times h$ in the flow and wall-normal direction and an immersed cylinder with diameter $d = h/2$, where h is the channel height (see figure 5). The domain is discretized with 120×60 nodes in the flow and wall-normal directions. The bulk Reynolds number is set to $Re_b = U_b h/\nu_f = 40$ and $Re_b = U_b h/\nu_f = 50$ in two different test cases. The drag coefficient obtained by Sahin et al. [16] is then compared to that obtained from the present simulation. The results are reported in table 1 where $C_d = D/(0.5\rho_f D U_b^2)$. It can be noted that present methodology overestimates the Drag Coefficient of around a 10%. It is well known that multi-direct IBM tends to increase the effective size of the bodies and this explains the higher drag found in this highly confined geometry. Some methods

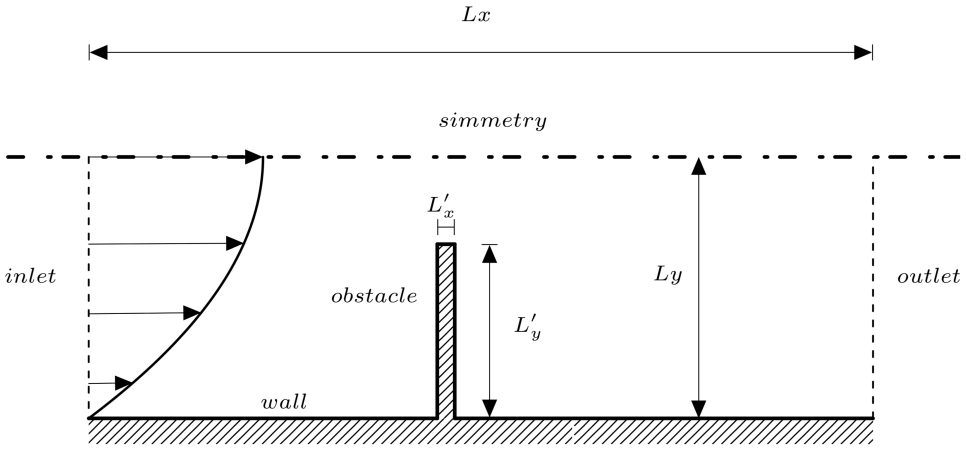

Figure 6: Schematic of the computational domain for the bending plate invested by the channel flow.

have been proposed to mitigate this issue (retraction) [13] that we aim to implement in next future.

Re	40	50
$C_{d,1}$	5.5	5.0
$C_{d,2}$	6.0	5.5

Table 1: Comparison between the drag coefficient of the cylinder obtained by Sahin et al. [16], $C_{d,1}$ and the results of the present test, $C_{d,2}$, at two different bulk Reynolds number.

In order to further proof the capabilities of the proposed methodology an additional test have been carried out. The simulation reproduces the bending of a 2D plate immersed in a channel and subjected to the hydrodynamic forces induced by the incident flow. The geometry of the domain is shown in figure 6. The domain extends for $L_x = 4.5\ 10^{-2}m \times L_y = 1.5\ 10^{-2}m$ in the flow and wall-normal directions respectively and is dicretized by an Eulerian grid of $N_x = 180 \times N_y = 60$ nodes. The mechanical properties of the material are set to $E = 7300Pa$, $\rho_s = 2440kg/m^3$, $k_d = 10^5 N\ s/m$. The bending plate extends for $L'_y = 10^{-2}m$ in the wall-normal direction and has a thickness of $L'_x = 10^{-3}m$. The plate is represented by a set of 4000 peridynamic particles distributed according to a Cartesian equispaced mesh ($N'_x = 20 \times N'_y = 200$) in the reference configuration. The m ratio between peridynamic particle spacing (in the reference configuration) and peridynamic horizon is set to $m = \Delta/\delta = 3$. The bulk Reynolds number is set to $Re_b = U_b L'_y/\nu_f = 125$. The fluid properties are set to $\rho_f = 1000kg/m^3$ and $\nu_f = 1.6\ 10^{-6}m^2/s$. The IBM forcing is computed using 1 peridynamic particle every 5 particles located on the solid-fluid interface. Figure 7 shows the velocity field in the channel at four different time steps. The bending of the plate due to the action of the hydrodynamic forces is evident and some release of vorticity from the plate tip can be observed during the transient. The present findings appear qualitatively correct and promising for the future work where we aim to provide quantitative validations on FSI problems even in reproducing crack formation

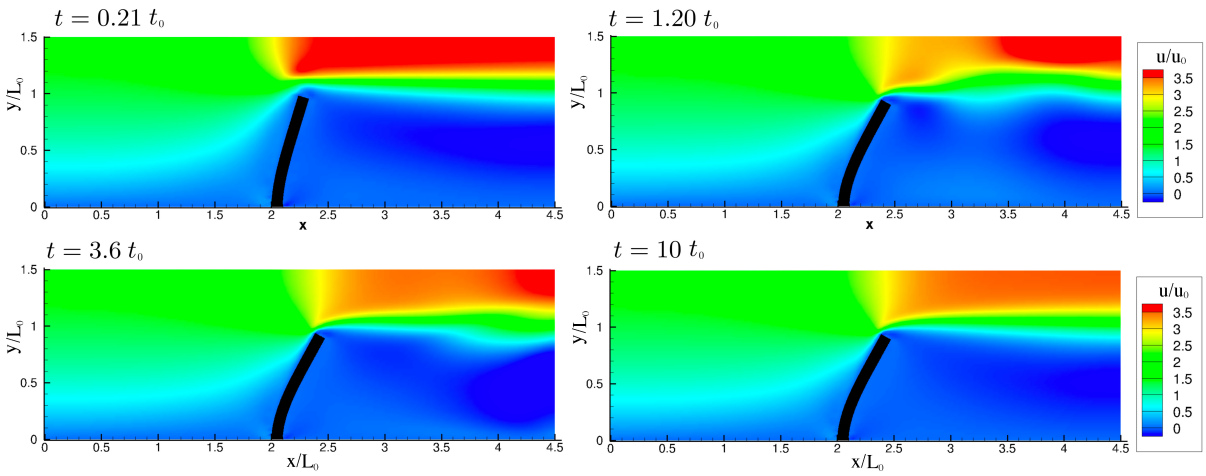

Figure 7: Contours of the x component of the velocity field, u, at four different time steps. Quantities are non-dimensional with the reference length scale being $L_0 = L'_y$, $U_0 = U_b$ and $t_0 = L'_y/U_b$.

within the fluid flow.

4 CONCLUSION

The present paper provides an overview of a novel numerical method for fluid structure interaction problems based on Navier-Stokes equations coupled with peridynamic equations through a multidirect IBM algorithm. In the peridynamic formulation of continuum mechanics the interaction among material points is described by integral equations. When crack formation is accounted for, local theory may present issues due to singularity of derivatives in partial differential equations. Conversely, the use of the peridynamic integral equations can avoid the insurgency of this kind of problem when crack formation occurs. The described methodology has been implemented into a massively parallelized Fortran code based on MPI and OpenMP directives. The paper provides validation tests and preliminary results for different solid and fluid configurations. The peridyanamic model has shown good reliability in reproducing solid media fracture and crack branching. Also the fluid solver and the IBM algorithm has been tested with good overall results. A simulation of a solid plate inserted in a channel and subjected to hydrodynamic forces induced by the incident flow has been performed. Qualitative non-steady results are presented. The methodology is potentially capable of reproduce solid rupture within fluids.

ACKNOWLEDGEMENTS

The authors M. Zaccariotto and U. Galvanetto would like to acknowledge the support they received from University of Padua under the research project BIRD2017 NR.175705/17. The authors F. Dalla Barba and F. Picano would also like to acknowledge the CINECA award under the ISCRA C initiative (project ExPS HP10C6CSU6), for the availability of high performance computing resources and support.

REFERENCES

[1] Hou, G., Wang, J. and Layton, A. Numerical methods for fluid-structure interaction - a review. *Communications in Computational Physics*. (2012) **12(2)**:337-377.

[2] Afonso, F., Vale, J., Oliveira, ., Lau, F. and Suleman, A. A review on non-linear aeroelasticity of high aspect-ratio wings. *Progress in Aerospace Sciences*. (2017) **89**:40-57

[3] Lambert, R. A., Picano, F., Breugem, W. P. and Brandt, L. Active suspensions in thin films: nutrient uptake and swimmer motion. *Journal of Fluid Mechanics*. (2013) **733**:528-557.

[4] Heil, M. and Hazel, A. L. Fluid-structure interaction in internal physiological flows. *Annual review of fluid mechanics*. (2011) **43**:141-162.

[5] Hattori, G., Trevelyan, J., Augarde, C. E., Coombs, W. M. and Aplin, A. C. Numerical simulation of fracking in shale rocks: Current state and future approaches. *Archives of Computational Methods in Engineering*. (2017) **24(2)**:281-317.

[6] Silling, S. A. Reformulation of elasticity theory for discontinuities and long-range forces. *Journal of the Mechanics and Physics of Solids*. (2000) **48(1)**:175-209.

[7] Dipasquale, D., Zaccariotto, M. and Galvanetto, U. Crack propagation with adaptive grid refinement in 2D peridynamics. *International Journal of Fracture*. (2014) **190(1-2)**:1-22.

[8] Silling, S. A. and Lehoucq, R. B. Peridynamic theory of solid mechanics. *Advances in applied mechanics*. (2010) **44**:73-168.

[9] Ha, Y. D. and Bobaru, F. Studies of dynamic crack propagation and crack branching with peridynamics. *International Journal of Fracture*. (2010) **162(1-2)**:229-244.

[10] Zaccariotto, M., Luongo, F. and Galvanetto, U. Examples of applications of the peridynamic theory to the solution of static equilibrium problems. *The Aeronautical Journal*. (2015) **119(1216)**:677-700

[11] Le, Q. V. and Bobaru, F. Surface corrections for peridynamic models in elasticity and fracture. *Computational Mechanics*. (2017) **16(5)**:1-20.

[12] Silling, S. A. and Askari, E. A meshfree method based on the peridynamic model of solid mechanics. *Computers & structures*. (2005) **83(17-18)**:1526-1535.

[13] Breugem, W. P. A second-order accurate immersed boundary method for fully resolved simulations of particle-laden flows. *Journal of Computational Physics*. (2012) **231(13)**:4469-4498.

[14] Roma, A. M., Peskin, C. S., and Berger, M. J. An adaptive version of the immersed boundary method. *Journal of computational physics*. (1999) **153(2)**:509-534.

[15] Kim, J., Moin, P. and Moser, R. Turbulence statistics in fully developed channel flow at low Reynolds number. *Journal of fluid mechanics*. (1987) **177**:133-166.

[16] Sahin, M. and Owens, R. G. A numerical investigation of wall effects up to high blockage ratios on two-dimensional flow past a confined circular cylinder. *Physics of Fluids*. (2004) **16(5)**:1305-1320.

[17] Costa, P. A FFT-based finite-difference solver for massively-parallel direct numerical simulations of turbulent flows. *arXiv preprint* (2018) **arXiv**:1802.10323.